

## SYNOPSIS

**Title:** A Pilot Study on Modeling and Management of Hurricane-Accelerated Saltwater Encroachment in Coastal Aquifers

### **Problem and Research Objectives**

This research studies the potential saltwater intrusion acceleration in East Baton Rouge (EBR) Parish relating to potential groundwater rise at south of the Baton Rouge Fault due to hurricane-induced sea level rise. In EBR, there are fourteen freshwater aquifers, which are composed of sediment from very fine to coarse sand and pea- to cobble-size gravel (Meyer and Turcan, 1955, p. 21-47). Thirteen of the aquifers were originally named according to their general depth in the Baton Rouge industrial district (Meyer and Turcan, 1955, p. 12-13). Most of the aquifers have been reported the saltwater intrusion problem for more than fifty years due to excessive groundwater withdrawal. In this study, we focus on the "1,500-foot" sand aquifer, which is a major source of drink water for the Capital Area (East Baton Rouge, West Baton Rouge, East Feliciana, West Feliciana, and Pointe Coupee Parishes). Groundwater withdrawal from the "1,500-foot" sand began in 1927 (Torak and Whiteman, 1982, Table 4). In 2001, the groundwater was withdrawn with 14.5 Mgal/d in EBR (Don Dial, Capital Area Ground Water Conservation Commission (CAGWCC), written communication 2002 cited in Griffith and Lovelace, 2003). From 1940 to 2001 water levels has declined about 160 ft at well EB-168, located near the pumping center southeast of the industrial district in Baton Rouge.

The Baton Rouge Fault represents an important hydrogeologic feature. Due to the throw-down at the south side of the fault, the "1,500-foot" sand (north) connects to the "1,200-foot" sand (south). Recent studies show that the Baton Rouge Fault acts as a leaky barrier, which does not completely block the saltwater encroachment from the south side of the fault. The large cone of depression in the northern area of the fault has induced saltwater encroachment across the fault toward the pumping centers in the "1,500-foot" sand, which previously contained freshwater. Tomaszewski (1996, p. 9) showed that saltwater was present in the "1,500-foot" sand north of the fault around an area of 3.88km<sup>2</sup> in the vicinity of the Acadian Thruway in Baton Rouge. To better understand the saltwater intrusion problem around the fault, the research overriding objective aims to develop a saltwater intrusion model for the "1,500-foot" sand in East Baton Rouge Parish. We will test different levels of groundwater head rise at the south of the Baton Rouge Fault to simulate the potential sea level rise from Gulf of Mexico.

### **Methodology**

#### **1. Data Collection for "1,500-Foot" Sand Groundwater Flow Model Development**

The study area shown in Figure 1 extends about 300 km<sup>2</sup> and includes the major part of the Baton Rouge metropolitan area. To develop the regional groundwater model, we have collected 706 groundwater observation records from 18 observation wells (see Figure 1a) for the period from January 1990 to December 2004 (15 years) through the USGS National Water Information System website. These 18 head observation wells are all in the "1,500-foot" sand of Baton Rouge Area [12115BR] north of the fault. The well EB-780A was used to determine the groundwater head in the "1,200-foot" sand for the southern boundary condition. The monthly pumping data from the 16 production wells (see Figure 1b) was provided by the CAGWCC.

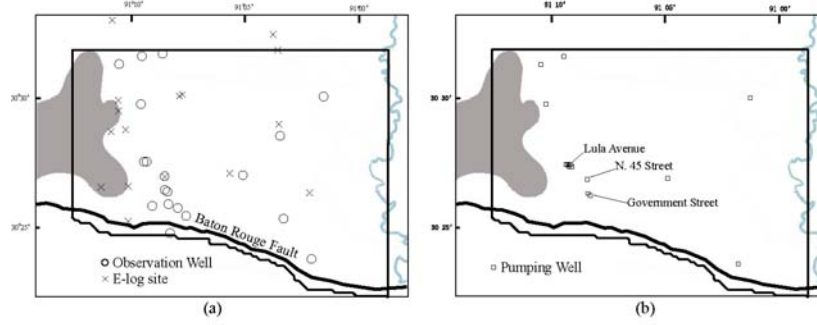


**Figure 1:** The study area. (a) The location of groundwater head observation wells and E-log wells. (b) The location of production wells.

We also obtained electrical resistivity data from 21 E-log wells (see Figure 1a) from USGS Water Resources Division in Louisiana. We analyzed the 21 resistivity readings and obtained the thickness of the “1,500-foot” sand as well as the average formation resistivity ( $R_0$ ). The 21 thickness data were used to construct the aquifer structure. Moreover, we used the Archie’s law to interpret the formation factor ( $F = R_0/R_w$ ) into the porosity (Archie 1942):

$$R_0 = a \Phi^{-m} R_w \quad (1)$$

where  $\Phi$  is the sand porosity. The two parameters  $a$  and  $m$  are the pore geometry coefficient and the cementation factor, respectively. Typically, the pore geometry coefficient  $a$  varies between 0.62 and 2.45, and the value of cementation factor  $m$  has a range between 1.08 and 2.15 depending on the formation type (Asquith and Gibson 1982). Once the porosity was estimated, we used the Kozeny-Carmen equation (Carmen 1956) to estimate pointwise hydraulic conductivity, which relates to the formation factor:

$$K = \frac{\gamma_w}{180\mu_w} \frac{(R_0/R_w)^{-1/m} a^{3/m}}{\left((R_0/R_w)^{1/m} - a^{1/m}\right)^2} d_e^2 \quad (2)$$

The groundwater temperature in the “1,500-foot” sand was reported as  $30^\circ\text{C}$ . The formation water resistivity was assumed to be  $R_w = 12.7$  ohm-m. The water specific weight  $\gamma_w = 9.771$  KN/m<sup>3</sup> and the dynamic viscosity  $\mu_w = 7.97 \times 10^{-4}$  N.s/m<sup>2</sup> were used in this study. The average effective particle diameter  $d_e = 0.22$  mm was calculated from the USGS sieve analysis data (Meyer and Turcan, 1955, page 40).

In this study, we developed a two-dimensional groundwater flow model using MODFLOW. In the next section, we estimated the pore geometry coefficient and the cementation factor in the Archie law. We also estimated storage coefficient (storativity) and hydraulic characteristic (HC) of the horizontal flow barrier (the fault). The hydraulic characteristic represents the hydraulic conductivity per unit width of the Baton Rouge Fault.

## 2. Groundwater Model Development

### 2.1 Parameter Estimation

In this study, we considered three interpolation methods (natural neighbor interpolation method (NN), inverse distance method (ID), and ordinary kriging method (OK)) as the initial step to depict hydraulic conductivity (K) heterogeneity based on the 21 pointwise K values at the E-log

sites. Given an interpolation method, Table 1 lists the estimated parameters through the inverse method.

**Table 1:** The Estimated Parameter Values.

Interpolation Method	Pore Geometry (a)	Cementation Factor (m)	Specific Storage (S <sub>s</sub> )	Fault Hydraulic Characteristic (HC)	Fitting Residual $\sum_j (h_j - h_j^{obs})^2$
NN	0.81926	2.0433	2.24E-05	0.0006920	2065.03
ID	0.81819	2.0391	2.13E-05	0.0001921	1378.05
OK	0.79657	2.0790	2.26E-05	0.0006736	1898.79
Average	0.81134	2.0538	2.21E-05	0.0005191	

The ID method has the best fit to the groundwater head observations with the fitting residual 1378.05. The identified parameter ( $a$ ,  $m$ ,  $S_s$ , and HC) values using three different interpolation methods are close to each other. We used the averaged identified parameter values in Table 1 to further the identification of hydraulic conductivity using the generalized parameterization (GP) method in section 2.3.

## 2.2 Bayesian Model Averaging on Hydraulic Conductivity Estimation

This study adopted the Bayesian model averaging (BMA) method (Draper, 1995; Hoeting et al., 1999) to consider multiple parameterization methods. Let a set of parameterization methods  $\Theta = \{\theta^{(p)}; p=1,2,\dots\}$  be considered to describe the hydraulic conductivity heterogeneity for the region. BMA provides a way to consider multiple parameterization methods through a weighted average of the conditional inferential distribution. Here, the ‘‘model’’ is referred to the parameterization method. If  $\Delta$  is a predicted quantity (scalar or vector) of interest, e.g., hydraulic conductivity, given available data  $\mathbf{D}$ , e.g., observed groundwater heads, the conditional inferential distribution  $\Pr(\Delta | \mathbf{D})$  given by BMA is

$$\Pr(\Delta | \mathbf{D}) = \sum_p \Pr(\Delta | \mathbf{D}, \theta^{(p)}) \Pr(\theta^{(p)} | \mathbf{D}) \quad (3)$$

where  $\Pr(\Delta | \mathbf{D}, \theta^{(p)})$  represents the conditional probability of the predicted quantity given the data and a parameterization method.  $\Pr(\theta^{(p)} | \mathbf{D})$  is the posterior probability of a parameterization method given the data. Consider the equal prior probability to all of the selected parameterization methods. According to the Bayes rule,  $\Pr(\theta^{(p)} | \mathbf{D})$  is

$$\Pr(\theta^{(p)} | \mathbf{D}) = \Pr(\mathbf{D} | \theta^{(p)}) / \sum_j \Pr(\mathbf{D} | \theta^{(j)}) \quad (4)$$

where  $\Pr(\mathbf{D} | \theta^{(p)})$  is the likelihood of the parameterization method. The conditional probability of the predicted quantity  $\Pr(\Delta | \mathbf{D}, \theta^{(p)})$  is approximated to  $\Pr(\Delta | \mathbf{D}, \theta^{(p)}, \hat{\boldsymbol{\beta}}^{(p)})$ , where  $\hat{\boldsymbol{\beta}}^{(p)}$  is the maximum likelihood estimation (MLE) of the parameters  $\boldsymbol{\beta}^{(p)}$  embedded in the parameterization method  $\theta^{(p)}$  (Draper, 1995). The conditional expectation of the predicted quantity is:

$$\mathbb{E}[\Delta | \mathbf{D}] = \sum_p \mathbb{E}[\Delta | \mathbf{D}, \theta^{(p)}] \Pr(\theta^{(p)} | \mathbf{D}) \quad (5)$$

The conditional covariance of the predicted quantity is:

$$\begin{aligned} \text{Cov}[\Delta | \mathbf{D}] &= \sum_p \text{Cov}[\Delta | \mathbf{D}, \theta^{(p)}] \Pr(\theta^{(p)} | \mathbf{D}) \\ &+ \sum_p \left( \mathbb{E}[\Delta | \mathbf{D}, \theta^{(p)}] - \mathbb{E}[\Delta | \mathbf{D}] \right) \left( \mathbb{E}[\Delta | \mathbf{D}, \theta^{(p)}] - \mathbb{E}[\Delta | \mathbf{D}] \right)^T \Pr(\theta^{(p)} | \mathbf{D}) \end{aligned} \quad (6)$$

The first term at the right side of Eq.(6) represents the within-parameterization covariance for individual parameterization methods. The second term represents the between-parameterization covariance.

### 2.3 Generalized Parameterization for Hydraulic Conductivity Estimation

This study adopted the generalized parameterization method (Tsai and Yeh, 2004; Tsai, 2006) to overcome the inflexibility problem in the traditional parameterization method:

$$\pi_{GP}(\mathbf{x}_0 | \mathbf{x}^{data}) = \sum_{\substack{j=1 \\ j \neq k(\mathbf{x}_0)}}^m \phi_j \left( \pi_j - \pi_{k(\mathbf{x}_0)} \right) \beta_j + \pi_{k(\mathbf{x}_0)} \quad (7)$$

where  $\pi_{GP}$  is an estimator for the hydraulic conductivity field. We considered  $\pi = \ln K$ , the logarithmic value of hydraulic conductivity.  $\beta_m = \{\beta_j, j=1, 2, \dots, m\}$  are the data weighting coefficients of the  $m$  sample sites, which values are bounded between 0 and 1. The Voronoi tessellation (VT) was used as a zonation method in Eq. (7). Readers are referred to Tsai (2006) for detailed explanation on Eq. (7) and the GP method. The conditional covariance using GP for a pair of two locations  $\mathbf{x}_p$  and  $\mathbf{x}_q$  is (Tsai, 2006):

$$\begin{aligned} \text{Cov}_{GP}[\mathbf{x}_p, \mathbf{x}_q | \mathbf{x}^{data}] &= \sum_{i \neq k(\mathbf{x}_p)}^m \sum_{j \neq k(\mathbf{x}_q)}^m \beta_i^p \beta_j^q \phi_i^p \phi_j^q R(\mathbf{x}_i, \mathbf{x}_j) - \sum_{i \neq k(\mathbf{x}_p)}^m \beta_i^p \phi_i^p R(\mathbf{x}_i, \mathbf{x}_q) \\ &- \sum_{j \neq k(\mathbf{x}_q)}^m \beta_j^q \phi_j^q R(\mathbf{x}_p, \mathbf{x}_j) + R(\mathbf{x}_p, \mathbf{x}_q) \end{aligned} \quad (8)$$

where  $R(\square)$  is the function of the semivariograms.

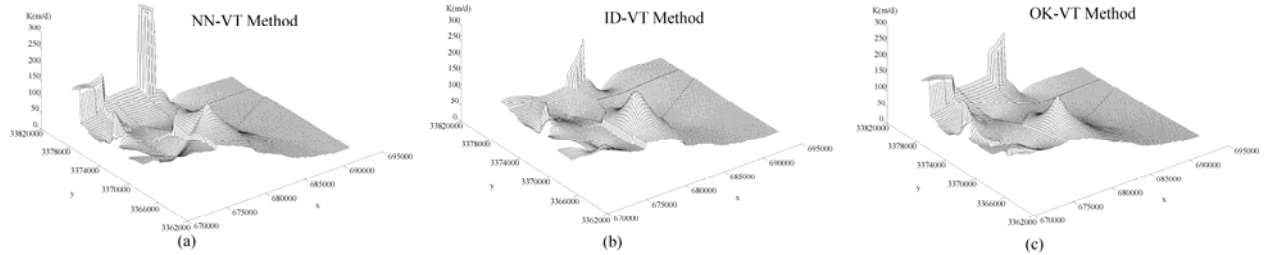


**Figure 2:** The identified hydraulic conductivity distributions using three GP methods (a) NN-VT, (b) ID-VT, and (c) OK-VT.

The optimal data weighting coefficients in each method were identified through the inverse method. Figure 2 shows and identified hydraulic conductivity distributions using three GP methods.

A scale factor  $\alpha = 3/\sqrt{706}$  was considered in the BMA in order to avoid overkilling good interpolation methods (Tsai and Li, 2007) when we combined the three K distributions in Figure 2. The scaled Bayesian information criterion (SBIC) was used as the multiplication of the scale factor and BIC to calculate the posterior probabilities (Eq.(4)). The groundwater head variance

$\sigma_h^2$  was estimated from the fitting residuals based on the four parameterization methods (NN, ID, OK, and VT). Table 2 lists the identified results using the optimal data weighting coefficients.

**Table 2:** The GP and BMA Results.

GP methods	NN-VT	ID-VT	OK-VT	BMA
$Q = \sum_j [(h_j - h_j^{obs}) / \sigma_h]^2$	481.64	438.76	464.97	441.21
SBIC	310.84	306	308.96	
$\Delta$ SBIC	4.84	0	2.96	
Posterior Probability, $\Pr(\theta^{(p)}   \mathbf{D})$	6.75%	75.96%	17.29%	
tr(Cov)	5344.5	5574.2	5172.7	5666.6

The ID-VT method has the lowest weighted fitting residual,  $Q = 438.76$ . Using the BMA, we have  $\Lambda = \pi^{data} = \ln K^{data}$  and  $\mathbf{D} = \mathbf{h}^{obs}$ . We found that ID-VT has the highest posterior probability 75.96% according to Eq.(4). NN-VT is relatively insignificant to the hydraulic conductivity estimation due to the low posterior probability. Using Eq.(5), BMA obtains the hydraulic conductivity distribution shown in Figure 3(a). The groundwater head distribution for April 2001 is shown in Figure 3(b) using the K distribution in Figure 3(a).

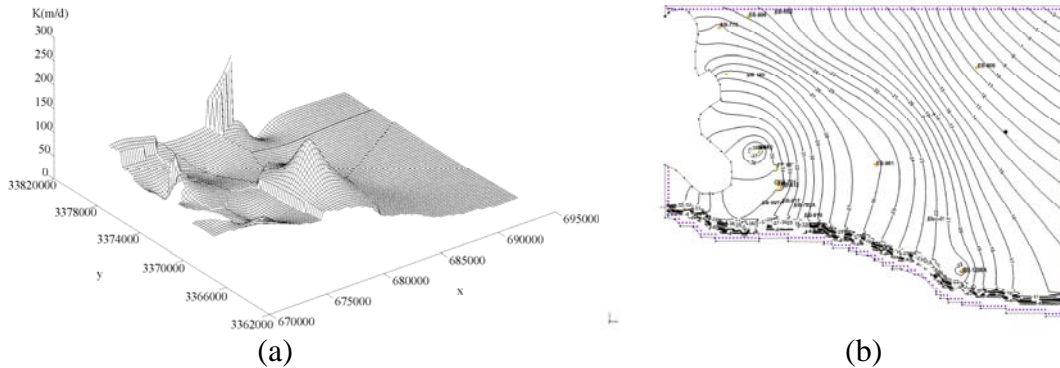


**Figure 3:** (a) The hydraulic conductivity distribution using BMA. (b) The groundwater head distribution for April 2001.

The uncertainty of the estimated hydraulic conductivity was calculated based on the trace of the conditional covariance matrix using Eq.(8). Table 2 shows that OK-VT has the lowest estimation uncertainty. However, the estimation uncertainties from the three GP methods and the BMP method are close to each other. The conditional variances of the hydraulic conductivity using Eq.(6) are shown in Figure 4. The within-variance is much higher than the between-variance.

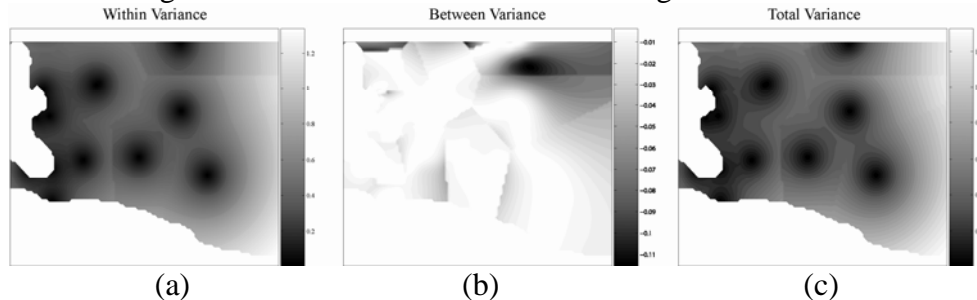


**Figure 4:** The conditional variance distributions for (a) the within-variance, (b) the between variance, and (c) the total variance.

## 2.4 Hydraulic Characteristic (HC) Estimation of Baton Rouge Fault

Another approach to estimate the hydraulic characteristic (HC) of the Baton Rouge Fault is to consider the influence of the groundwater heads at EB-917 on those at EB-780A through the fault. EB-780A and EB-917 are separated by the Baton Rouge Fault with a distance of 2,003 meters shown in Figure 5(a). Again, EB-780A screens the "1,200-foot" sand aquifer and EB-917 screens the "1,500-foot" sand. These two sands are partially connected at the fault plane. We considered a one-dimensional groundwater flow problem as shown in Figure 5(a), where we set EB-917 as a time-varied constant head boundary condition. We gave a no-flow boundary at the other end, which is far from the EB-780A and has no effect on the identification result. We identified the HC value of the fault to be  $0.000155 \text{ day}^{-1}$ . The calculated groundwater heads against the observed heads at EB-780A are shown in Figure 5(b). This HC value is close to that identified by the ID method and is in the same order of the magnitude to the average HC in Table 1. It is noted that due to lack of data a homogenous HC throughout the fault was considered in the groundwater model.

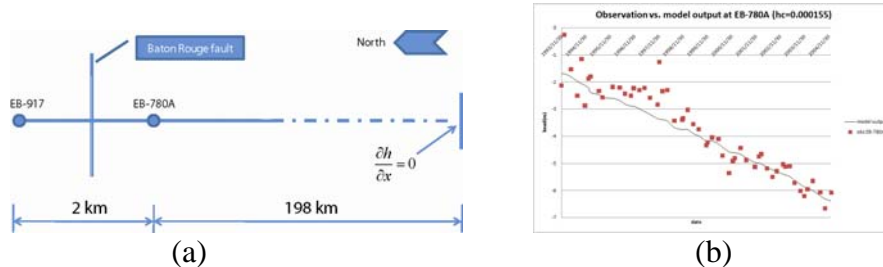


**Figure 5:** (a) The one-dimensional groundwater model. (b) The calculated vs. and observed groundwater head data at EB-780A.

## Principal Findings and Significance

### 1. The Connector Well, EB-1293

The groundwater model also incorporated the effect of the connector well, EB-1293. The connector well was operated in 1998 as an initial test of a recharge barrier to mitigate saltwater encroachment in the "1,500-foot" sand. CAGWCC installed EB-1293 between the municipal supply wells on Government Street and the freshwater-saltwater interface in the "1,500-foot" sand. The connector well, EB-1293, connects the "800-foot" and "1,500-foot" sands such that "800-foot" sand recharges groundwater into "1,500-foot" with a recharge rate around 500 gallons per minute (CAGWCC Newsletter, January 2002). The groundwater model is able to investigate the effectiveness of the connector well on raising the potentiometric surface around EB-1293 and deflect the advance of the saltwater away from the municipal supply wells at the Government Street.

In the first step, we used EB-1293 groundwater data from USGS as a time-varied constant head boundary condition in the model. Figure 6(a) shows a significant over-predicted groundwater head in EB-917 after the connector well head was added to the model. We suspected that the real EB-1293 groundwater data might not be as high as reported. Instead, we considered EB-1293 as a recharge well with a constant recharge rate  $2200 \text{ m}^3/\text{d}$ . In Figure 6(b), the model results show no significant differences between the calculated and observed head data in EB-917. Again, a

constant drift (around 7 meters) between the calculated and observed groundwater heads at EB-1293 shown in Figure 6(c) implies that a systematic recording error or a datum error might occur in the EB-1293 data. Nevertheless, the groundwater flow model shows that the connector well does raise the groundwater head around it. In the next section, we demonstrate the potential that the connector well is able to mitigate saltwater intrusion in the “1,500-foot” sand.

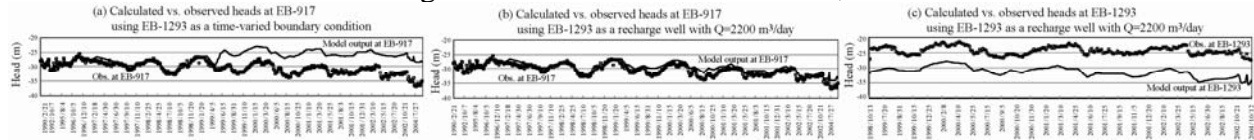


**Figure 6:** (a) Calculated vs. observed heads at EB-917 using EB-1293 as a time-varied head boundary condition. (b) Calculated vs. observed heads at EB-917 using EB-1293 as a recharge well with 2200 m<sup>3</sup>/day recharge rate. (c) Calculated vs. observed heads at EB-1293 using EB-1293 as a recharge well with 2200 m<sup>3</sup>/day recharge rate.

## 2. Saltwater Intrusion Simulation for 90 Years

At this point, a calibrated groundwater flow model has been completed. In the next step, we want to simulate saltwater intrusion based on the 15-year simulated groundwater heads between year 1990 and 2004 in order to understand the basic mechanism how saltwater intrudes the “1,500-foot” sand. We didn’t calibrate the transport model, but assumed the porosity to be 0.3, longitudinal dispersivity to be 75 m, and the ratio of transverse to longitudinal dispersivities to be 0.1 in the transport model. We used MT3DMS to simulate the saltwater intrusion. We recognized the density effect on the groundwater flow and will consider using SEAWAT in the future study.

The initial salt concentration at January 1990 was assumed to be clean in the northern area of the fault and 1000 ppm (parts per million) of salinity in the southern region of the fault. Figure 7(a) shows the initial salt concentration distribution. We repeated the 15-year groundwater heads six times in order to simulate a 90-year saltwater intrusion. From the simulation results in Figure 7(b)-(g), we observe the following points:

- (1) The saltwater has strong lateral transport along the Baton Rouge Fault once it crosses the fault due to the huge cone of depression formed by the production wells at Lula Avenue.
- (2) The salt dispersion width at the region east of EB-918 is around 850 meters from the fault and is almost unchanged after 30 years simulation. This also implies the strong lateral transport along the fault and weak dispersion northward in this region.
- (3) The salt accumulates at two spots. One spot is at 600 meters the southeast of EB-807A. From this spot, a higher salt concentration migrates clockwise across EB-807A toward Lula Avenue pumping center. The other spot is at 2200 meters southwest of EB-807A.
- (4) The 100 ppm isochlor (the front line) migrates to a production well adjacent to the observation well EB-1295A within 45 years.
- (5) The 100 ppm isochlor first touches down EB-918 and few years later it touches EB-807A. Due to the clockwise movement of the salt along the fault from the east, the concentrations in EB-807A and EB-918 are similar.
- (6) The 100 ppm isochlor touches EB-917 and EB-792A almost at the same time. The simulation results show that the concentrations in EB-917 and EB-792A are similar due to the clockwise movement of the salt along the fault.
- (7) After 90 years, the 100 ppm isochlor reaches the Lula Avenue pumping center.

(8) Figure 7(e) shows a salt movement toward the Government Street pumping center within 60 years. As shown in Figure 7 (f) and (g), the connector well does push the saltwater away from south of the Government Street pumping center.

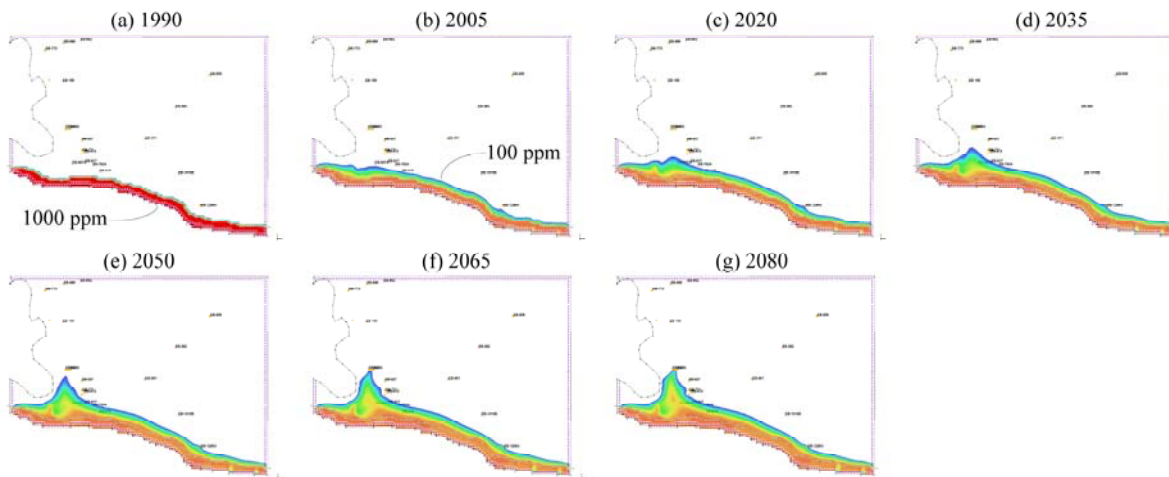


**Figure 7:** The 90-year saltwater intrusion simulation results.

In summary, although the saltwater intrusion is close to the Government Street pumping center, the simulation results show that saltwater will reach the Lula Avenue pumping center before it reaches Government Street. More observation wells are suggested at the west of EB-807A to monitor the saltwater mitigation.

### 3. Saltwater Intrusion Enhancement with Groundwater Rise at South of the Fault

To simulate the hurricane-induced groundwater rise at south of the fault, we artificially raised the groundwater head at the south boundary with additional 2, 4, and 6 meters high and rerun the 90-year saltwater intrusion model. We simulated the worst-case scenarios that the raised heads would stay for 90 years.

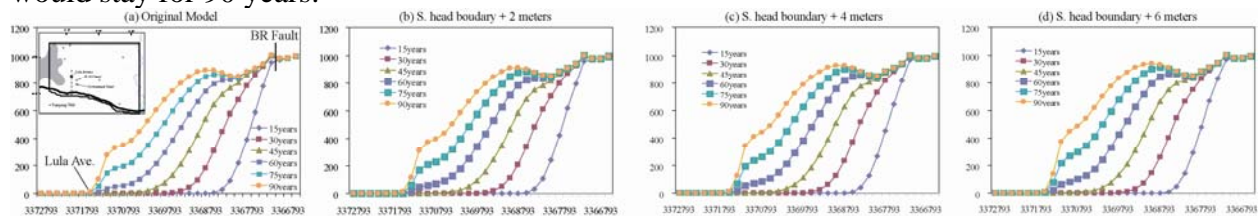


**Figure 8:** Breakthrough curves for different south groundwater head boundary conditions.

Figure 8 shows the saltwater encroachment along a vertical line (see Figure 8a) through the Lula Avenue pumping center. Figure 9 compares the breakthrough curves at 15 and 90 years. We conclude that the breakthrough curves are not significantly changed for the first 15 years when groundwater heads were raised. However, additional intrusion of salt concentration is observed after 30 years. Nevertheless, the arrival time of saltwater to Lula Avenue does not change significantly even though the groundwater head increases south of the fault.

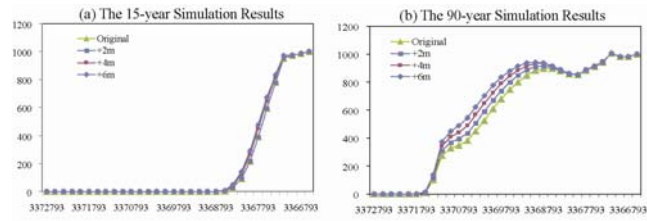


**Figure 9:** Breakthrough curve comparisons for different south groundwater head boundary conditions at (a) 15 years and (b) 90 years.